Published in IET Electric Power Applications
Received on 18th December 2009
Revised on 14th May 2010
doi: 10.1049/iet-epa.2009.0305

ISSN 1751-8660

Practical approach to model electric motors for electromagnetic interference and shaft voltage analysis

F. Zare

School of Engineering Systems, Queensland University of Technology, Gardens Point Campus, 2 George Street, GPO Box 2434, Brisbane, QLD 4001, Australia
E-mail: f.zare@qut.edu.au

Abstract: This study presents a practical method to find a high-frequency model of AC machine in order to predict leakage current and shaft voltage. A voltage-source inverter with hard switches generates pulse width modulated voltage with high dv/dt and common-mode voltage, which causes leakage current and shaft voltage due to stray capacitances in an electric motor. At fundamental frequency (a few hundred hertz), an equivalent circuit of an electric motor consists of inductances and resistances without considering stray capacitances. This study presents a practical approach in extracting high-frequency parameters of an electric motor for leakage current and shaft voltage analysis. Input impedance (magnitude and phase values) of several configurations of an AC motor is measured using a network analyser. All capacitive couplings between windings, stator and rotor are extracted based on theoretical analysis and measurement results. Simulations are compared with test results to verify the proposed method and model.

1 Introduction

Electromagnetic compatibility is an important issue in modern power electronic systems. As switching speed of power devices used in power modules is increased, electromagnetic interference (EMI) becomes a major problem in power electronic circuits. Since more than 60% of the world's energy is used to drive motors, it is important to characterise and predict electromagnetic emission behaviour of the motor drive systems.

Modern power electronic drives are large complex systems consisting of a power supply, filter, rectifier, inverter and motor as shown in Fig. 1*a*. In these motor drive systems, high-frequency leakage currents generated by high dv/dt of hard and fast switches flow to a ground wire through stray capacitors between windings and the motor frame.

Fig. 1*b* shows a three-phase inverter where (V_{ao}, V_{bo}, V_{co}) and (V_{an}, V_{bn}, V_{cn}) are the leg voltages and phase voltages of the three-phase inverter, respectively. V_{no} is the voltage between the neutral point and the ground (common-mode voltage). The six-switch combination of this inverter has eight permitted switching vectors which have been shown in Fig. 1*c*. According to Fig. 1*b*, the three-leg voltages of the inverter can be calculated as follows

$$\begin{cases} V_{ao}(t) = V_{an}(t) + V_{no}(t) \\ V_{bo}(t) = V_{bn}(t) + V_{no}(t) \\ V_{co}(t) = V_{cn}(t) + V_{no}(t) \end{cases} \quad (1)$$

By adding two sides of (1)

$$V_{ao}(t) + V_{bo}(t) + V_{co}(t) = V_{an}(t) + V_{bn}(t) + V_{cn}(t) + 3 \times V_{no}(t) \quad (2)$$

It is obvious that the sum of the three-phase voltages is equal to zero ($V_{an}(t) + V_{bn}(t) + V_{cn}(t) = 0$). Therefore the common-mode voltage can be calculated as

$$V_{no}(t) = \frac{V_{ao}(t) + V_{bo}(t) + V_{co}(t)}{3} \quad (3)$$

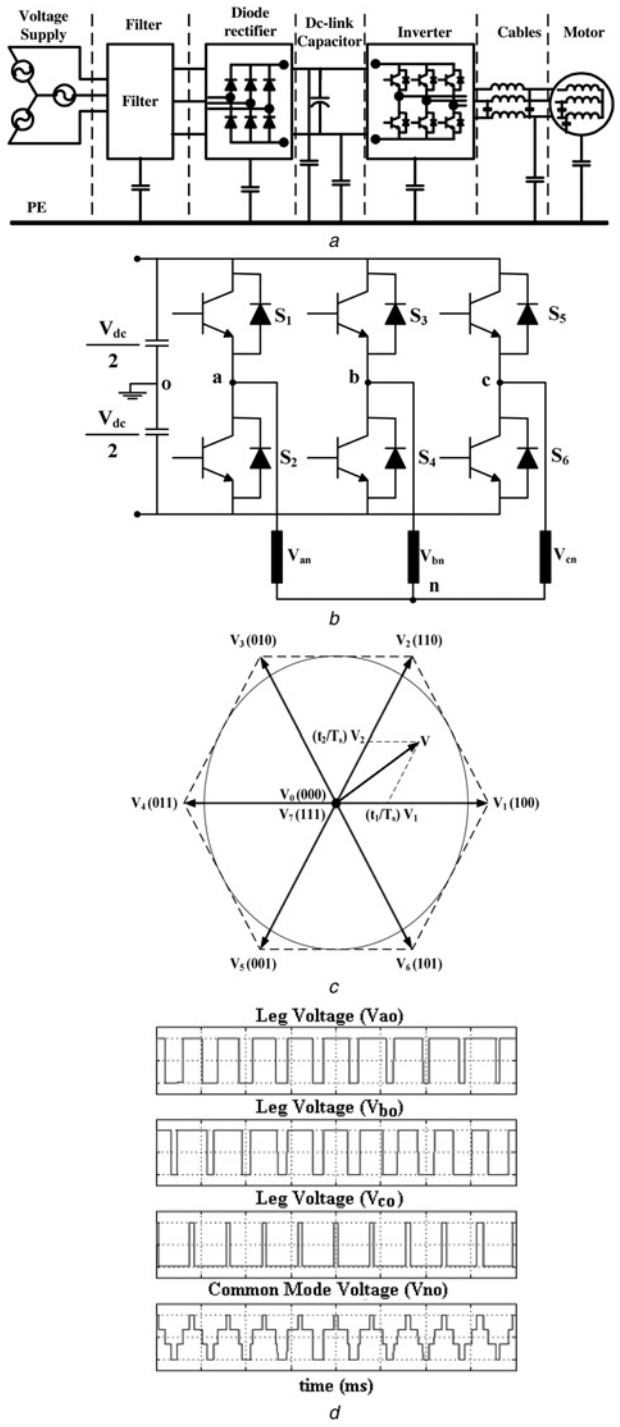

Figure 1 *A modern power electronic drive*

a Motor drive system connected to grid
b Circuit diagram of an inverter
c Eight switching vectors
d Legs and common-mode voltage waveforms

One of the inherent characteristics of pulse width modulation (PWM) techniques is the common-mode voltage which is defined by switching pattern. By using an appropriate switching pattern, the common-mode voltage level can be controlled. The switching states of the inverter, the leg voltages and the common-mode voltage are shown in Fig. 1*d* and given in Table 1. In a three-phase motor drive system, common-mode voltage – generated by an inverter – is a main source of shaft voltage which causes bearing current.

Shaft voltage is influenced by various factors such as capacitive couplings between different parts of the machine structure, configuration of the main supply and switching states in PWM pattern [1, 2]. Different techniques to reduce common-mode voltage based on PWM methods for three-phase voltage-source inverters have been proposed by authors. In [3], new modulation techniques – near-state PWM and active zero-state methods – are analysed considering advantages and disadvantages of the modulation methods as overall superior methods. This paper aids in the selection and application of appropriate modulation methods in inverter drives with low common-mode voltage requirements. In [4], a simple technique is proposed to select switching states to synthesise the desired voltage vectors for multilevel inverter to reduce common-mode voltage.

Understanding of common-mode EMI issues such as generation and mitigation of EMI as well as modelling and test methods are presented in [5]. A high-frequency behaviour of an induction motor with regard to the impact of magnetic core selection, parasitic interturn and skin effects of windings is investigated in [6].

Recently, some techniques are presented to mitigate shaft voltage and bearing currents in doubly-fed induction generators based on modulation techniques to cancel out shaft voltage [7]. An approach is used in [8, 9] to measure high-frequency parameters for shaft voltage analysis and modelling of motor bearing currents.

It is important to find a high-frequency model of an AC motor to predict leakage current and shaft voltage in order to estimate EMI filter size at the beginning stage of a design. Selecting a good PWM technique and a proper and fast switching speed can reduce voltage/current harmonics and switching losses, respectively. On the other hand, these may increase shaft voltage and/or leakage current due to capacitive couplings in an AC motor. Thus, to select a proper switching time and PWM strategy, it is important to predict shaft voltage and leakage current which requires a good high-frequency model to analyse the motor. Different approaches have been developed to model AC motors for common-mode leakage current analysis by measuring capacitive coupling between windings and stator. In [10, 11], several approaches have been proposed to extract capacitive couplings for common-mode leakage current analysis. A high-frequency model of an induction motor has been proposed in [12, 13] to analyse common-mode and differential-mode emission noise. In this analysis, capacitive coupling between phases and between phases and rotor have not been considered for differential-mode noise and shaft voltage analysis. A low-voltage high-power AC motor drive system has been proposed to analyse

doi: 10.1049/iet-epa.2009.0305

Table 1 Switching states, leg voltages and common-mode voltage

Vector	S_1	S_3	S_5	V_{ao}	V_{bo}	V_{co}	V_{no}
$\boldsymbol{V}_1$	1	0	0	$\frac{V_{dc}}{2}$	$-\frac{V_{dc}}{2}$	$-\frac{V_{dc}}{2}$	$-\frac{V_{dc}}{6}$
$\boldsymbol{V}_2$	1	1	0	$\frac{V_{dc}}{2}$	$\frac{V_{dc}}{2}$	$-\frac{V_{dc}}{2}$	$\frac{V_{dc}}{6}$
$\boldsymbol{V}_3$	0	1	0	$-\frac{V_{dc}}{2}$	$\frac{V_{dc}}{2}$	$-\frac{V_{dc}}{2}$	$-\frac{V_{dc}}{6}$
$\boldsymbol{V}_4$	0	1	1	$-\frac{V_{dc}}{2}$	$\frac{V_{dc}}{2}$	$\frac{V_{dc}}{2}$	$\frac{V_{dc}}{6}$
$\boldsymbol{V}_5$	0	0	1	$-\frac{V_{dc}}{2}$	$-\frac{V_{dc}}{2}$	$\frac{V_{dc}}{2}$	$-\frac{V_{dc}}{6}$
$\boldsymbol{V}_6$	1	0	1	$\frac{V_{dc}}{2}$	$-\frac{V_{dc}}{2}$	$\frac{V_{dc}}{2}$	$\frac{V_{dc}}{6}$
$\boldsymbol{V}_7$	1	1	1	$\frac{V_{dc}}{2}$	$\frac{V_{dc}}{2}$	$\frac{V_{dc}}{2}$	$\frac{V_{dc}}{2}$
$\boldsymbol{V}_0$	0	0	0	$-\frac{V_{dc}}{2}$	$-\frac{V_{dc}}{2}$	$-\frac{V_{dc}}{2}$	$-\frac{V_{dc}}{2}$

EMI [14] without considering high-frequency parameter of the AC motor. A new approach to find high-frequency transfer function of a motor drive system is proposed in [15, 16]. In this case, the proposed model is only used for frequency-domain analysis and conducted emission noise and it is not possible to separate parameters for shaft voltage analysis or time-domain simulations.

This paper addresses a comprehensive and a practical method to extract most important high-frequency parameters (capacitive couplings) of an AC motor based on input impedance measurement of different configurations. In the proposed method, it is recommended to estimate the behaviour of the motor in a frequency range, in which the motor acts as a capacitive or an inductive load according to phase value of the input impedance. Based on different configurations, there are different frequency ranges (low or high-frequency ranges) in which phase value of the input impedance is almost -90° (capacitive load) or $+90^\circ$ (inductive load) over that frequency range. This paper presents a new model of an AC motor to be used for common-mode and differential-mode conducted emission noise and shaft voltage analysis.

2 Modelling of an electric motor for EMI and shaft voltage analysis

A classical model of an electric motor is used for steady-state and dynamic analysis at fundamental frequency (up to few hundred hertz) and it cannot be used for shaft voltage and EMI analysis (in kHz or MHz range) due to the existence of stray capacitances between windings, rotor and stator. This paper presents a practical approach to extract all parameters (such as capacitive couplings) in an AC motor based on measuring input impedance across different terminals in a broad frequency range using a network analyser.

Fig. 2*a* shows a comprehensive high-frequency model of an AC motor consisting of

C_{ws}: capacitive coupling between windings and stator;

C_{rs}: capacitive coupling between rotor and stator;

C_{wr}: capacitive coupling between windings and rotor;

C_w: capacitive coupling between turns of a winding;

C_{ww}: capacitive coupling between windings;

L: winding inductance;

R_{loss}: resistance to model losses.

Fig. 2*b* shows a circuit diagram similar to the one shown in Fig. 2*a*, but without the rotor which gives a better configuration to find C_w, C_{ws}, R_{loss} and L. Figs. 2*c* and *d* show the cross-sections of the AC motor with and without the rotor, respectively. Input impedance of five different configurations in an AC motor are measured using a network analyser in a broad frequency range in order to extract high-frequency parameters based on magnitude and phase values.

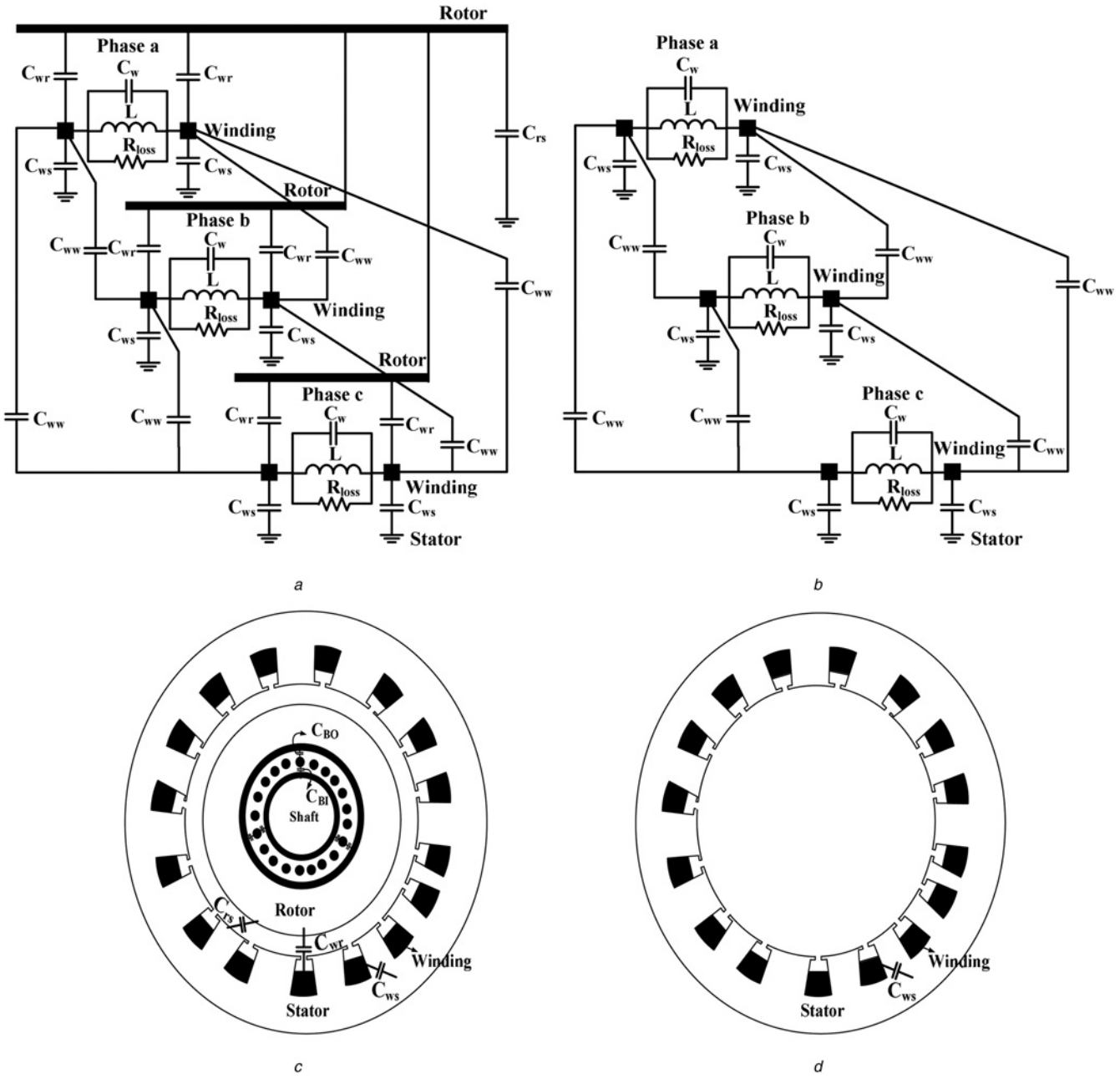

Figure 2 *Comprehensive high-frequency model of an AC machine:*

a With rotor
b Without rotor
Cross-section of an AC motor
c With rotor
d Without rotor

A simple method with analysis and equations to extract the high-frequency parameters is presented in this paper.

2.1 Test 1: input impedance across windings (either T_1 or T_2) and stator (motor frame) to extract C_{ws}

This test is performed to extract the capacitive coupling between the phase windings and the stator based on the configuration shown in Fig. 2*b*. In order to simplify the configuration, the three phases are connected in parallel assuming that the windings of the motor are in a star form (Fig. 3*a*). In this case, C_{ww}s are removed from the model due to short circuits between the phases. The input impedance – phase and magnitude values – across one terminal of the phases (either T_1 or T_2) and the stator (motor frame) is measured in terms of frequency using a network analyser. At low-frequency range – below the resonant frequency ($f < 70$ kHz according to Fig. 7) – when an equivalent impedance of R_{loss} and L is less than

doi: 10.1049/iet-epa.2009.0305

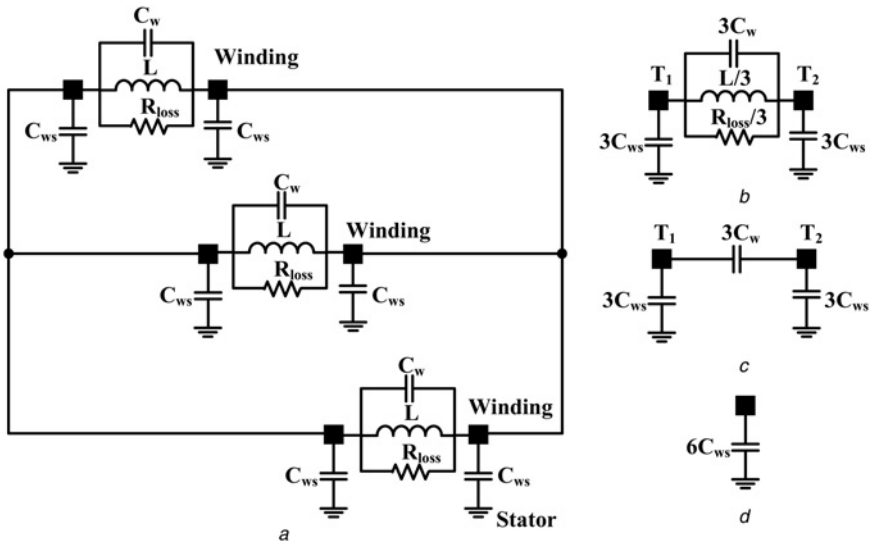

Figure 3 *AC motor without rotor*

a Three phases are connected in parallel
b Equivalent circuit diagram
c High-frequency model
d Low-frequency model

C_w and C_{ws} impedances, the impedance across T_1 and T_2 is very low compared to other capacitive impedances and we assume these terminals are connected to each other. In this case, the input impedance of this configuration will be capacitive (Fig. 3*d*) – in which the phase value is close to -90° – and C_{ws} can be calculated as follows

$$C_{test1\_low} = 3C_{ws} + 3C_{ws} = 6C_{ws} \tag{4}$$

We can also calculate the capacitance value at high-frequency range ($f > 300$ kHz according to Fig. 7) when the impedance of R_{loss} and L is much higher than the impedance of C_w (Fig. 3*c*) and the phase value is close to -90° (Fig. 7*b*). As $C_{ws} \gg C_w$, thus

$$C_{test1\_high} = 3C_{ws} + \frac{3C_w \times 3C_{ws}}{3C_w + 3C_{ws}} \simeq 3C_{ws} + 3C_w \simeq 3C_{ws} \tag{5}$$

This analysis shows that the capacitive coupling between the winding and the stator can be calculated in two different ways but it is recommended to calculate C_{ws} based on (4) which is more accurate than (5).

2.2 Test 2: impedance of windings to extract C_w, R_{loss} and L

The second measurement is based on Fig. 3*a*, but the impedance across terminals T_1 and T_2 is measured. The configuration is shown in Fig. 4*a*. The impedance of C_w and C_{ws} is much higher than the impedance of L and R_{loss} at low-frequency range ($f < 70$ kHz according to Fig. 7) and it can be simplified as an inductive and a resistive load as shown in Fig. 4*b*.

At this frequency range when the phase value is close to 90°, we can extract the inductance value based on magnitude and frequency values. The inductance value is almost constant with respect to frequency while the resistance value is changed due to losses. The main point is that R_{loss} is a function of frequency and it can be modelled as a non-linear load but it makes the model very complex. Another alternative is to choose a correct value for R_{loss}, with a performance close to experimental results. In order to define a simple and linear circuit to model an AC motor for EMI and shaft voltage analysis, it is recommended to calculate R_{loss} at the first resonant frequency.

At a high-frequency range ($f > 300$ kHz according to Fig. 7), the phase value is close to -90°, which presents a capacitive load. In this case, the impedance of L and R_{loss}

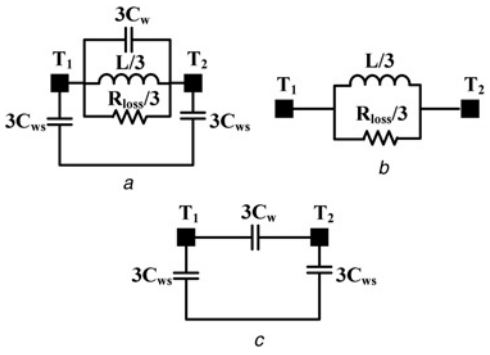

Figure 4 *Impedance of windings*

a Circuit diagram based on Fig. 3*a* and input impedance across terminals T_1 and T_2
b Low-frequency model
c High-frequency model

is much higher than the equivalent impedance of C_w and C_{ws}, as shown in Fig. 4*c*. Thus, the capacitance value can be calculated as follows

$$C_{test2} = 3C_w + \frac{3C_{ws} \times 3C_{ws}}{3C_{ws} + 3C_{ws}} = 3C_w + \frac{3}{2}C_{ws} \quad (6)$$

As we found C_{ws} is based on (4), C_w can be extracted based on (6) as follows

$$C_w = \frac{C_{test2} - (3/2)C_{ws}}{3} \quad (7)$$

The inductance, L can also be calculated based on the resonant frequency of L and C_{test2} as follows

$$L = \frac{3}{(2\pi f)^2 C_{test2}} \quad (8)$$

2.3 Test 3: input impedance across rotor and stator to extract C_{rs} and C_{wr}

The next configuration is based on Fig. 2*a* – the AC motor with the rotor – and all the three phases are connected in parallel assuming that the windings of the motor are in a star form. Similar to the above circuit diagram, C_{ww}s are removed from the model due to short circuits between the phases as shown in Fig. 5*a*. A simplified model of this configuration is shown in Fig. 5*b*. At a low-frequency range ($f < 70$ kHz according to Fig. 9) – when the impedance of L and R_{loss} is much less than other capacitive impedances – this configuration can be simplified to three capacitors shown in Fig. 5*c*. Thus, this circuit diagram can be used to measure the input impedances across, stator and rotor and rotor and windings in order to extract C_{rs} and C_{wr}, respectively. Thus

$$C_{test3} = C_{rs} + \frac{6C_{wr} \times 6C_{ws}}{6C_{wr} + 6C_{ws}} \quad (9)$$

As $C_{ws} \gg C_{wr}$, thus

$$C_{test3} \simeq C_{rs} + 6C_{wr} \quad (10)$$

In this configuration, we need to electrically isolate the rotor from the frame in order to measure C_{rs}. In a static situation, the rotor shaft which is connected to two ball bearings at both sides of the rotor are connected electrically to the stator through the outer race, metallic balls and inner race of the ball bearings. Thus, using an insulator to separate either the outer race or the inner race of ball bearing from the stator (motor frame) can help to measure the input impedance across the rotor and the stator.

Although C_{wr} is much less than C_{rs} and (10) gives an approximate value for C_{rs}, we need to consider both C_{rs} and C_{wr} parameters in this equation and find another equation to extract C_{wr} precisely. Thus, the next test is to measure the input impedance across the windings and the rotor according to the circuit diagram shown in Fig. 5*c*.

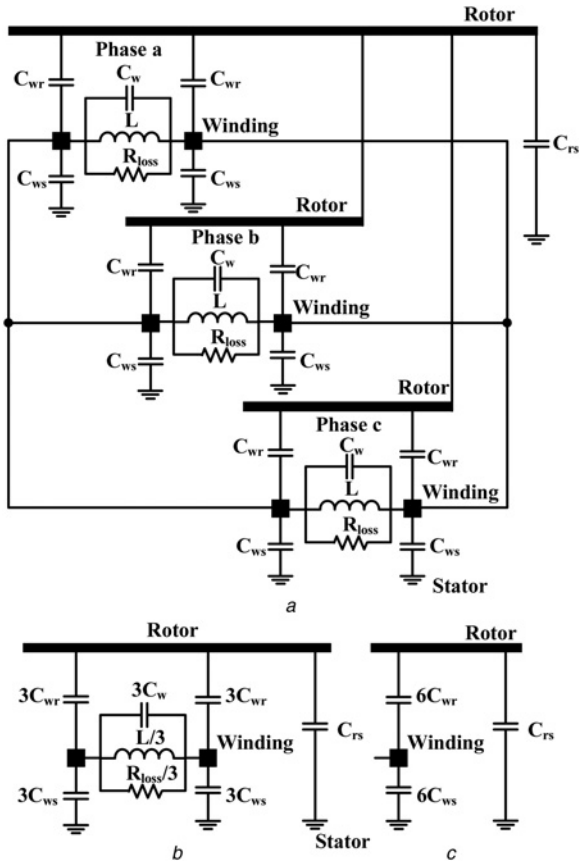

Figure 5 *AC motor with rotor*

a Three phases are connected in parallel
b Equivalent circuit diagram
c Low-frequency model

2.4 Test 4: input impedance across windings and rotor to extract C_{rs} and C_{wr}

In this test, the input impedance across one of the winding terminals and the rotor is measured. As shown in Fig. 5*c*, the capacitor, $6C_{ws}$ is in series with C_{rs} and they are in parallel with $6C_{wr}$. Thus, the equivalent capacitance can be calculated as follows

$$C_{test4} = 6C_{wr} + \frac{C_{rs} \times 6C_{ws}}{C_{rs} + 6C_{ws}} \quad (11)$$

As we found C_{ws} from the previous test and analysis (4), we can find the two unknown parameters (C_{rs} and C_{wr}) based on (10) and (11) as follows

From (10), we can find C_{wr} in terms of C_{test3} and C_{rs}.

$$6C_{wr} = C_{test3} - C_{rs} \quad (12)$$

doi: 10.1049/iet-epa.2009.0305

Substituting (12) in (11) yields

$$C_{test4} = C_{test3} - C_{rs} + \frac{C_{rs} \times 6C_{ws}}{C_{rs} + 6C_{ws}} \quad (13)$$

Thus, we can sort the above equation in terms of C_{rs} as follows

$$C_{test4} - C_{test3} = \frac{-C_{rs}^2 - C_{rs} \times 6C_{ws} + C_{rs} \times 6C_{ws}}{C_{rs} + 6C_{ws}} \quad (14)$$

Thus

$$C_{rs}^2 - (C_{test3} - C_{test4})C_{rs} - 6(C_{test3} - C_{test4})C_{ws} = 0 \quad (15)$$

From (15), we can find C_{rs} in terms of the test results (C_{test3} and C_{test4}) and C_{ws}

$$C_{rs} = \frac{(C_{test3} - C_{test4}) \pm \sqrt{(C_{test3} - C_{test4})^2 + 24(C_{test3} - C_{test4})C_{ws}}}{2} \quad (16)$$

It is obvious that C_{rs} has a positive value, thus the only answer for C_{rs} is given by

$$C_{rs} = (C_{test3} - C_{test4}) + \sqrt{\frac{(C_{test3} - C_{test4})^2 + 24(C_{test3} - C_{test4})C_{ws}}{2}} \quad (17)$$

2.5 Test 5: input impedance across the phases to extract C_{ww}

This test is important in finding capacitive couplings between the phases which have significant impact on conducted emission noise – differential mode – due to dv/dt generated by the PWM voltage. In a real case, to make the motor windings, one side of the winding is placed into one slot and the winding is twisted with other windings at the end of the rotor sides, in order to put the other side of the winding into another slot. This configuration creates capacitive coupling between phases due to the end windings, even in an AC motor with one winding per each slot.

To be able to extract these capacitive couplings, the rotor is removed and two phases (in this analysis, phase 'a' and 'b') are connected in parallel (Fig. 6*a*) and the impedance across phase 'c' (T_c) and these two phases (T_{ab}) is measured as shown in Fig. 6*b*. It is important to consider that the other side of the phases are not connected to each other which means C_{ww} between the phases 'a and b' and the phase 'c' exist at both sides of the windings. At a low-frequency range ($f < 80$ kHz according to Fig. 11), when the impedance of R_{loss} and L is much less than the other capacitive impedance, the model can be simplified as shown in Fig. 6*c*. In this case, $4C_{ws}$ is in series with $2C_{ws}$ and they are in parallel with $4C_{ww}$.

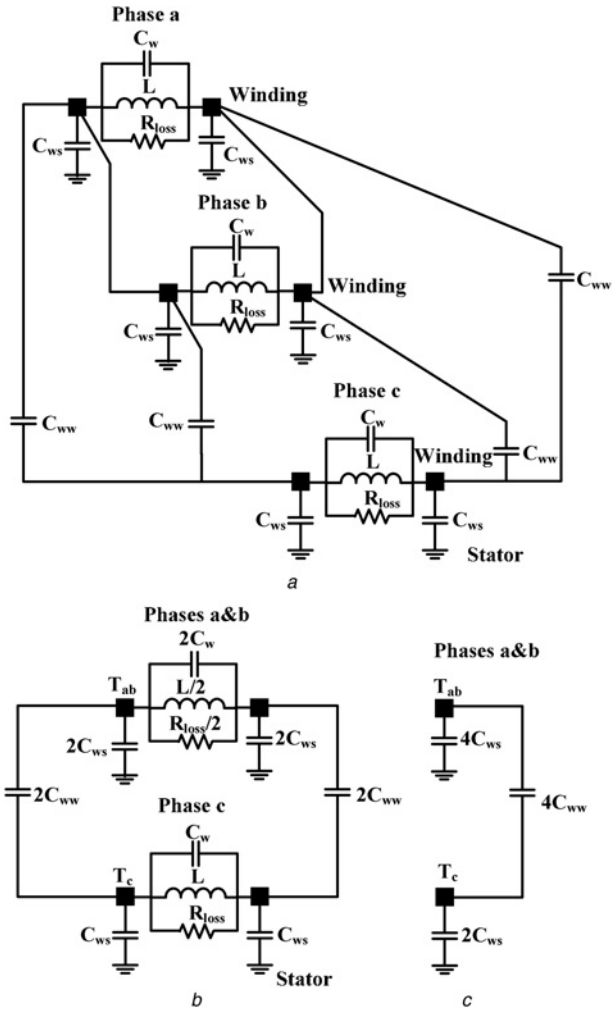

Figure 6 *AC motor without rotor*

a Two phases (a and b) are connected in parallel
b Equivalent circuit diagram
c Low-frequency model

$$C_{test5} = 4C_{ww} + \frac{4C_{ws} \times 2C_{ws}}{4C_{ws} + 2C_{ws}} = 4C_{ww} + \frac{4}{3}C_{ws} \quad (18)$$

3 Experimental results

According to the above test procedures, five tests have been performed to measure the input impedance magnitude and phase values across different terminals to extract high-frequency parameters based on the above equations. Simulations have been carried out based on the high-frequency parameters extracted from the above test results and circuit diagram shown in Figs. 2*a* and *b*. For a 5.5 kW

induction motor, the parameters are extracted as follows

$$C_{ws} = 495\,\text{pF}$$
$$R_{loss} = 10\,\text{k}\Omega$$
$$L = 3.54\,\text{mH}$$
$$C_{w} = 15\,\text{pF}$$
$$C_{rs} = 760\,\text{pF}$$
$$C_{wr} = 11.5\,\text{pF}$$
$$C_{ww} = 155\,\text{pF}$$

The input impedances (magnitude and phase values) of the two configurations (Figs. 3*b* and 4*a*) have been compared with the test results. Fig. 7*a* shows the test and simulation results associated with the input impedance magnitude across the terminal T_1 and the stator (motor frame) in terms of frequency. According to Fig. 7*b*, the phase value is −90 for the low-frequency range ($f < 70$ kHz) and the capacitive coupling has been extracted according to (4). The equivalent impedance of R_{loss} and L affects the input impedance for the frequency range of 70–200 kHz. As we have discussed and addressed in the above section, the resistance value has been extracted at the resonant frequency. Thus, at higher frequency range there is an error between the test and the simulation results – phase values – but it is not significant. In fact, in EMI and shaft voltage analysis the most important parameters are the capacitive couplings.

Fig. 7*c* shows the test and simulation results for the input impedance magnitude across terminals T_1 and T_2 in terms of frequency. According to the phase value shown in Fig. 7*d*, at the low-frequency range ($f < 70$ kHz) the phase value is around 90°, which shows an inductive load and the inductance value has been extracted based on both magnitude and phase values. The simulation and test results shown in Fig. 7 verify the proposed analysis as a reliable method to find an accurate model of an AC motor for EMI and shaft voltage analysis.

From the test results, L equals 3.54 mH based on the phase and magnitude values and 3.6 mH based on (8). The error between these two values is less than 1.7%, which shows a good validation for the proposed methods to calculate L in two different ways. As was mentioned in the above section, R_{loss} changes with respect to frequency and the selection of a proper value for R_{loss} is important. Fig. 8 shows the input impedance across terminals T_1 and T_2 for

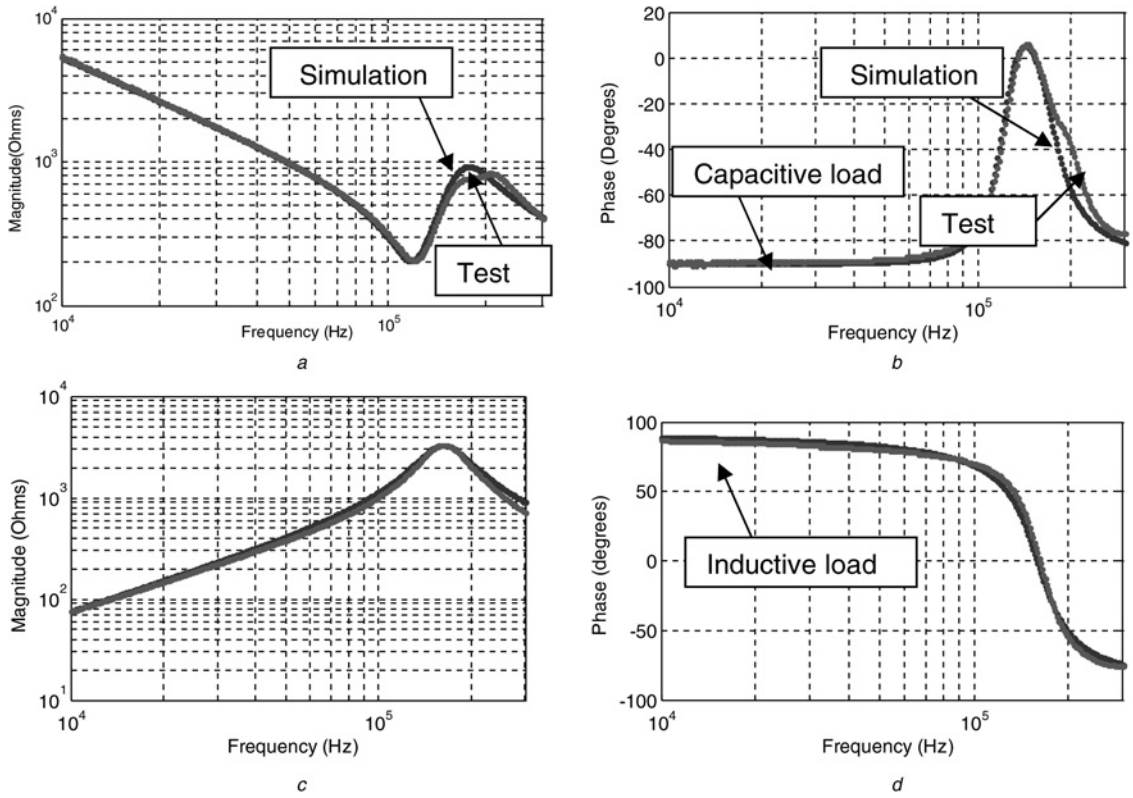

Figure 7 *Test and simulation results:*

a Magnitude
Input impedance across terminal T_1 and the stator
b Phase
Input impedance across terminals T_1 and T_2
c Magnitude
d Phase

doi: 10.1049/iet-epa.2009.0305

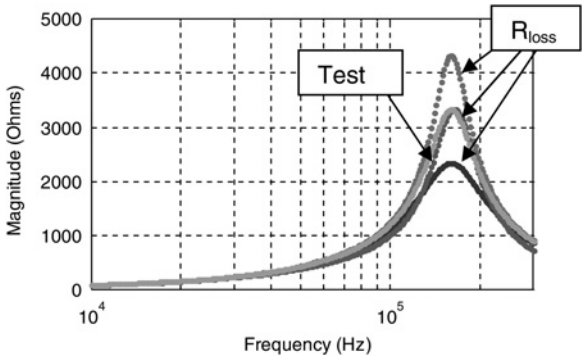

Figure 8 *Input impedance magnitude across terminals T_1 and T_2 (according to Fig. 4a) test result and simulation results with different R_{loss}*

three different R_{loss} values and the simulation results show the best value with minimum error can be found at resonant frequency, which means magnitude of the impedance at the resonant frequency presents the resistance value.

Fig. 9*a* shows the test result – capacitance values between the stator and the rotor in terms of frequency – in which the phase value is close to −90 for a broad frequency range (Fig. 9*b*) and presents a capacitive load for that frequency range. The result shows that the capacitance value is constant and C_{test3} is equal to 829 pF.

Fig. 10*a* shows the capacitance values between the winding and the rotor in terms of frequency extracted from the test result. At the low-frequency range ($f < 100$ kHz), the phase value is close to -90° (Fig. 10*b*) and the input impedance presents a capacitive load for this frequency range.

Using the tests results (C_{test3}, C_{test4}) and C_{ws}, calculated from the previous test, C_{rs} and C_{wr} can be found based on (17) and (12) and the results are 760 and 11.5 pF, respectively.

In the last test, phases 'a' and 'b' are connected in parallel and the input impedance between one terminal of phases 'a and b' and one terminal of phase 'c' is measured in terms of frequency. From the test result and as shown in Fig. 11, the phase value is close to -90° for the low-frequency range ($f < 40$ kHz), which presents a capacitive load. In this measurement, C_{test5} equals to 1280 pF for this frequency range and C_{ww} is calculated using (18) and the result is 155 pF.

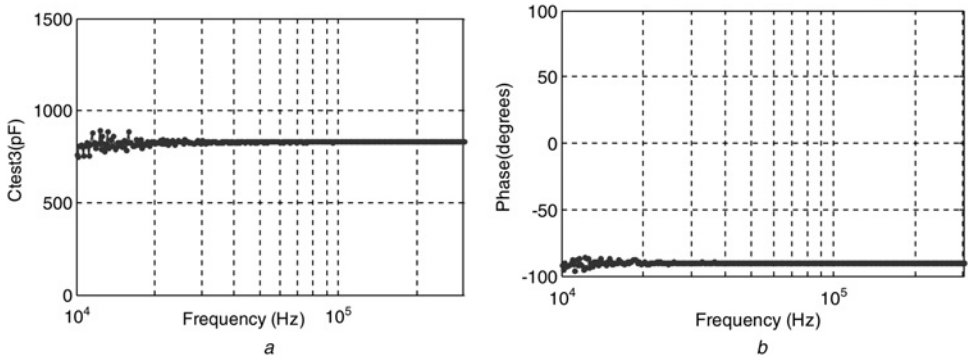

Figure 9 *Test results – according to the circuit diagram shown in Fig. 5b*

a Capacitance value between the rotor and the stator in terms of frequency
b Phase value

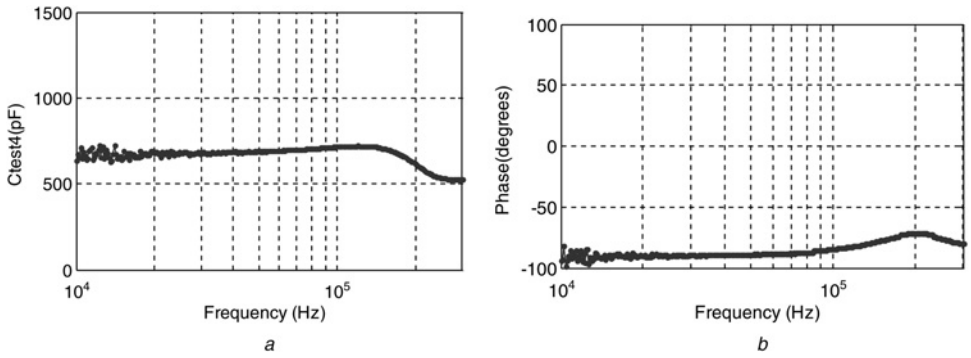

Figure 10 *Test results – according to the circuit diagram shown in Fig. 5b*

a Capacitance value between the windings and the rotor
b Phase value

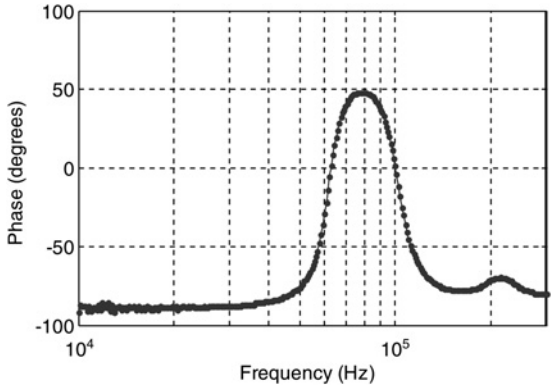

Figure 11 *Phase value of the input impedance in terms of frequency associated with the circuit diagram shown in Fig. 6b*

In this section, a comprehensive high-frequency model of 5.5 kW AC motor based on the proposed method is used to analyse shaft voltage. In this case, common mode and shaft voltage are measured for the 5.5 kW induction motor. According to the test results shown in Fig. 12*a*, the DC-link voltage is 500 V and the shaft voltage is 46 V.

In order to validate the proposed high-frequency model, a three-phase inverter is connected to the comprehensive high-frequency model (refer to Fig. 2*a*) with $V_{dc} = 500$ V. A PWM strategy is applied to the inverter to simulate a power converter connected to the induction motor in order to find the shaft voltage and common-mode voltage; the results are shown in Fig. 12*b*. The error between the simulation and the test results is very low which verifies the proposed method to extract the parameters such as the capacitive couplings.

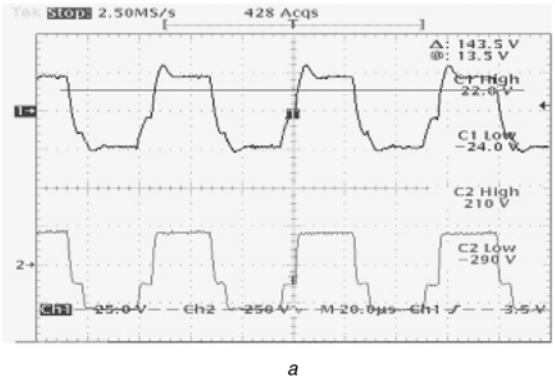

a

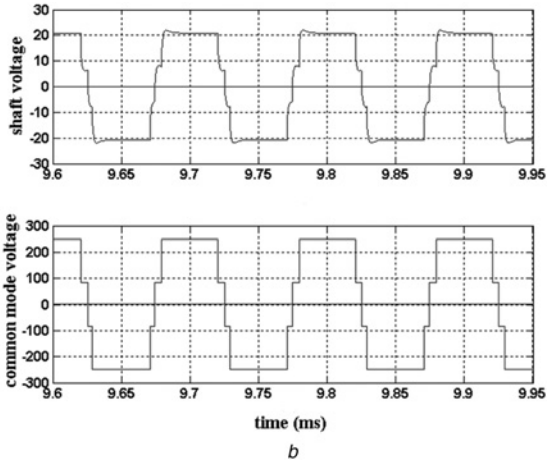

b

Figure 12 *Common mode and shaft voltage*

a Test result; simulation results
b With the comprehensive model (Fig. 2*a*)

4 Discussion

According to the above analysis and the test and simulation results, the circuit diagram shown in Fig. 2*a* can be simplified for different analysis as described below:

1. For shaft voltage analysis, as the frequency of the common-mode voltage waveform is almost three times of the frequency of the leg voltage waveform, thus the frequency of the common-mode voltage waveform is around 60 kHz for the leg switching frequency of 20 kHz. This means for the shaft voltage analysis we can use a simple model shown in Fig. 5*c* which is valid for the frequency range below 100 kHz. The simple high-frequency model of the motor drive is shown in Fig. 13*a* and the shaft voltage can be calculated as follows

$$V_{\text{shaft}} = \frac{6 \times C_{\text{wr}}}{6 \times C_{\text{wr}} + C_{\text{rs}}} \times V_{\text{no}} \tag{19}$$

In this case, the shaft voltage magnitude can be calculated based on the capacitive couplings C_{rs} and C_{wr} and the common-mode voltage, V_{no}. If the capacitive coupling between the winding and the rotor, C_{wr} is much less than the capacitive coupling between the rotor and the stator,

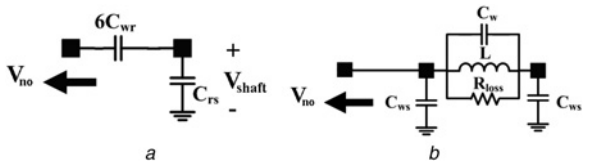

a *b*

Figure 13 *Simple model of an AC motor*

a Shaft voltage
b Common mode (leakage) current calculation

doi: 10.1049/iet-epa.2009.0305

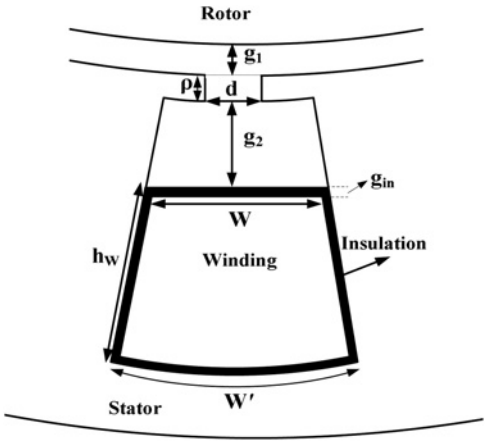

Figure 14 *Stator slot with different parameters*

C_{rs}, thus, (19) can be simplified to $V_{shaft} = \frac{6 \times C_{wr}}{C_{rs}} \times V_{no}$

- The common-mode voltage magnitude depends on the DC-link voltage and the switching patterns.

- C_{rs} depends on the effective surface between the rotor and the stator and the air-gap size.

- As shown in Fig. 14, the shape of the slot has a significant effect on C_{wr} and the shaft voltage.

2. For conducting emission noise analysis – both the common-mode and differential-mode noise – the circuit diagram shown in Fig. 2*b* can be used. The main reason is that C_{wr} is very small and has less effect on the leakage current generated by PWM voltage and dv/dt.

To predict only common-mode current (leakage current) magnitude, the circuit diagram shown in Fig. 13*b* can be used and a PWM voltage with different switching transient can be applied to analyse the effect of the switching transient time on the leakage current magnitude.

5 Conclusions

A comprehensive high-frequency model of an electric motor has been analysed in this paper. An impedance of a 5.5 kW induction motor has been measured in terms of frequency using a network analyser and the results have been used to extract the high-frequency parameters. One of the advantages of the high-frequency model of an electric motor is to analyse leakage current and shaft voltage due to dv/dt and common-mode voltage, respectively. According to (19), the ratio of C_{wr}/C_{rs} can be found by measuring the shaft voltage and the DC-link voltage but in this practical approach, we can predict the shaft voltage level before applying any PWM voltage across the motor. The model can be used to perform simulation to predict conducted emission noise and shaft voltage in order to have a better EMI filter design and define a proper PWM strategy. It is recommended to estimate the behaviour of the motor in a frequency range, when the motor acts as a capacitive or an inductive load according to the phase value of the impedance.

6 Acknowledgment

The author thanks the Australian Research Council (ARC) for the financial support for this project through the ARC Linkage Grant LP0774899.

7 References

[1] ALEXANDER L.J., ORITI G., LIPO T.A.: 'Elimination of common-mode voltage in three-phase sinusoidal power converters', *IEEE Trans. Power Electron.*, 1999, **14**, (5), pp. 982–989

[2] MEI C., BALDA J.C., WAITE W.P., CARR K.: 'Minimization and cancellation of common-mode currents, shaft voltages and bearing currents for induction motor drives'. IEEE 34th Annual, PESC'03, 2003

[3] HAVA M.A., UN E.: 'Performance analysis of reduced common-mode voltage PWM methods and comparison with standard PWM methods for three-phase voltage-source inverters', *IEEE Trans. Power Electron.*, 2009, **24**, (1), pp. 241–252

[4] MOHAN M.R., HIRALAL M.S.: 'Five-level diode clamped inverter to eliminate common mode voltage and reduce dv/dt in medium voltage rating induction motor drives', *IEEE Trans. Power Electron.*, 2008, **23**, (4), pp. 1598–1607

[5] SKIBINSKI G.L., KERKMAN R.J., SCHLEGEL D.: 'EMI emissions of modern PWM AC drives', *IEEE Ind. Appl. Mag.*, 1999, **5**, pp. 47–80

[6] MIRAFZAL B., SKIBINSKI G.L., TALLAM R.M.: 'Determination of parameters in the universal induction motor model', *IEEE Trans. Ind. Appl.*, 2007, **45**, (1), pp. 1207–1216

[7] SON Y.C., SUL S.K.: 'A new active common-mode EMI filter for PWM inverter', *IEEE Trans. Power Electron.*, 2003, **18**, (6), pp. 1309–1314

[8] CHEN S., LIPO T.A., FITZGERALD D.: 'Modelling of motor bearing currents in PWM inverter drives', *IEEE Trans. Ind. Appl.*, 1996, **32**, (6), pp. 1365–1370

[9] ADABI J., ZARE F., LEDWICH G., GHOSH A.: 'Leakage current and common mode voltage issues in modern ac drive systems' (AUPEC, Perth, Australia, 2007)

[10] BOGLIETTI A., CARPANETO E.: 'An accurate high frequency model of AC PWM drive systems for EMC analysis'. 36th IAS Annual Meeting, Conf. Record 2001 IEEE Industry Applications Conf., 2001, vol. 2, pp. 1111–1117

[11] ZARE F.: 'A high frequency modelling of electric motors for fast switching applications'. Tenth European Conf. on Power Electronics and Applications, September 2003

[12] CONSOLI G.O., TESTA A., JULIAN A.L.: 'Induction motor modelling for common mode and differential mode emission evaluation'. 31st IAS Annual Meeting, Industry Applications Conf., 1996, vol. 1, pp. 595–599

[13] MUETZE A., BINDER A.: 'Techniques for measurement of parameters related to inverter-induced bearing currents', *IEEE Trans. Ind. Appl.*, 2007, **43**, (5), pp. 1274–1283

[14] LAI J.S., HUANG X., CHEN S., NEHL T.W.: 'EMI characterization and simulation with parasitic models for a low-voltage high-current AC motor drive', *IEEE Trans. Ind. Appl.*, 2004, **40**, (1), pp. 178–185

[15] LUSZCZ J., MOSON I.: 'AC motor windings circuit model for common mode EMI currents analysis'. The 5th International Compatibility in Power Electronics (CPE) Conference, 29 May–1 June 2007, Gdansk, Poland

[16] JETTANASEN C., COSTA F., VOLLAIRE C., REVOL B., MOREL F.: 'Measurements and simulation of common mode conducted noise emissions in adjustable-speed ac drive systems'. 20th Int. Zurich Symp. on Electromagnetic Compatibility, January 2009, pp. 181–184

doi: 10.1049/iet-epa.2009.0305